Engineering Applications of Artificial Intelligence 142 (2025) 109978

Contents lists available at ScienceDirect

Engineering Applications of Artificial Intelligence

journal homepage: www.elsevier.com/locate/engappai

Unsupervised learning for motion correction and assessment in brain magnetic resonance imaging using severity-based regularized cycle consistency

Seuk Kim [a,1], Mohammed A. Al-masni [b,1], Seul Lee [a], Sunyoung Jung [a], Kyu-Jin Jung [a], Chuanjiang Cui [a], Sung-Min Gho [c], Young Hun Choi [d], Dong-Hyun Kim [a,*]

[a] Department of Electrical and Electronic Engineering, College of Engineering, Yonsei University, Seoul, Republic of Korea
[b] Department of Artificial Intelligence and Data Science, College of AI Convergence, Sejong University, Seoul, Republic of Korea
[c] Medical R&D Division, DEEPNOID, Seoul, Republic of Korea
[d] Department of Radiology, Seoul National University Hospital, Seoul, Republic of Korea

ARTICLE INFO

Keywords:
Motion artifact correction
Motion artifact assessment
Cycle consistency loss
Unsupervised deep learning
Rigid motion artifact

ABSTRACT

Magnetic resonance imaging is an important non-invasive diagnostic tool, yet is vulnerable to motion artifacts due to the long acquisition time. With the recent development of deep learning, numerous methods for improving motion artifacts have been proposed. Due to the difficulty in constructing paired datasets for motion artifact correction, various unsupervised learning-based models have emerged recently. Cycle-Consistent Generative Adversarial Network (CycleGAN), which is widely used as a base model for unsupervised learning, has ill-posed problem and high parameter complexity that poses limitations towards an unstable training process. To overcome these limitations, this paper proposes an unsupervised learning method for motion artifact correction and assessment by replacing one generator of CycleGAN with a motion artifact simulator and regularizing the cycle-consistency loss with a motion severity prior. In adopting this approach, the overall model's training complexity can be significantly reduced due to the decrease in the quantity of learnable parameters. Moreover, the calculation of the cycle-consistency loss becomes more stable, thereby addressing the inherent ill-posed problem of CycleGAN. As a result, the proposed method demonstrates superior performance quantitatively and qualitatively compared to existing motion artifact correction methods and succeeds in reconstructing clearer images qualitatively compared to supervised learning methods.

1. Introduction

1.1. Motion artifacts in MRI

Magnetic Resonance Imaging (MRI) is a widely used non-invasive diagnostic tool for imaging soft tissues without radiation exposure. However, subject movements during data acquisition can lead to various artifacts in reconstructed images (Zaitsev et al., 2015). Motion artifacts can be categorized into non-rigid and rigid types. Non-rigid motion, caused by physiological factors, includes involuntary deformation movements. This encompasses periodic and continuous movements such as respiration, cerebrospinal fluid (CSF) flow, and peristalsis as well as sudden involuntary movements such as swallowing and coughing (Godenschweger et al., 2016). Rigid motion, often due to intentional or unexpected movements, can affect all body parts, including brain scans, and is more prevalent in non-compliant subjects such as children or patients with degenerative diseases of the nervous system. In this case, the aspects of motion artifacts can vary slightly depending on the k-space data acquisition trajectory, in which ghosting artifacts are usually caused by sudden subject motion while blurring artifacts are typically the result of continuous subject motion (Lee et al., 2020; Shaw et al., 2020; Zaitsev et al., 2015).

With the advancement of MR hardware, spatial resolution and signal-to-noise ratio (SNR) have improved, but relatively long scan times have still made the images susceptible to motion artifacts. Thus, such motion artifacts, which compromise image quality and interpretation,

* Corresponding author.
E-mail address: donghyunkim@yonsei.ac.kr (D.-H. Kim).
[1] Authors equally contributed to this work.

https://doi.org/10.1016/j.engappai.2024.109978
Received 26 April 2024; Received in revised form 12 December 2024; Accepted 29 December 2024

may significantly impact on subsequent patient diagnosis in clinical. Hence, motion artifact correction strategies remain a critical issue in MR imaging.

1.2. Previous work

Prospective and retrospective methods are two different approaches for conventional motion artifact correction in MRI (Atkinson et al., 1997; Cordero-Grande et al., 2016; Haskell et al., 2018; Herbst et al., 2012; Tisdall et al., 2012; Vaillant et al., 2013). Prospective correction methods involve real-time monitoring of the subject motion during the scan, and then using this information to correct the motion artifacts in the image data. This is achieved by synchronizing the scan with the subject motion, such as starting the scan when the subject reaches a specific position. These prospective motion correction methods aim to overcome motion effects by directly acquiring additional information through real-time external recording. The most common example of a prospective method is the navigator-based correction, which uses a secondary signal, known as a navigator, to monitor the motion (Bosak and Harvey, 2001). Retrospective correction methods entail correcting the motion artifacts after the scan has been completed. This is accomplished by estimating the motion from the corrupted images and then applying a correction to the data. However, these conventional methods necessitate the use of extra scanning equipment, extend the duration of the scan, and involve extensive computation to estimate motion (Godenschweger et al., 2016).

In addition to prospective motion correction methods that monitor patient movement during scaning, several technologies mitigate noise and artifacts prior to MRI data acquisition. These include parallel imaging (Hewlett et al., 2024), which utilizes multiple receiver coils for simultaneous data acquisition, and compressed sensing (Wang et al., 2024), which accelerates the acquisition process by undersampling data points and reconstructing the full image. These technologies help reduce motion artifacts by shortening scan times. However, as the volume of MRI data continues to grow, post-processing methods (i.e., retrospective approaches) are expected to play an increasingly significant role in addressing artifacts, particularly in pediatric and neurodegenerative patients who are more prone to movement during scans.

With the recent advancement of deep learning, various techniques have been developed for motion correction in MRI. Specifically, motion correction methods based on deep convolutional neural networks (CNN) have been developed (Dou et al., 2019; Duffy et al., 2018; Johnson and Drangova, 2018; Kromrey et al., 2020; Küstner et al., 2019; Lee et al., 2024; Liu et al., 2020; Loizillon et al., 2024; Oh et al., 2024; Pawar et al., 2022). Tamada et al. developed a motion artifact reduction using CNN, known as MARC, which utilized a deep CNN with multiple convolutional layers and performed motion correction by computing the patch-wise loss (Tamada et al., 2020). Pawar et al. proposed a MoCoNet, which is designed based on the U-Net architecture (Pawar et al., 2018). Recently, a study presented a motion correction model that utilized cascaded U-Nets with self-assisted priors (Al-masni et al., 2022). The model proposed a method to utilize three-dimensional (3D) information using two-dimensional (2D) network. Additionally, a knowledge interaction framework was proposed, which collaboratively learns from the feature details of multiple corrupted echoes by sharing their features through common training parameters (Al-masni et al., 2023). Furthermore, methods using generative adversarial networks (GANs), in which generators and discriminators are trained through mutual deception, have been introduced. For example, MoCo-cGAN, a method of motion artifact correction using conditional GAN, has been proposed. This method consisted of 3D U-Net and 6-layer CNN, and performed motion correction effectively on 3D MRI. Additionally, MedGAN, an end-to-end framework that integrated a conditional adversarial framework, non-adversarial losses, and a CasNET generator architecture, was proposed for medical image translation tasks, such as PET-CT translation, MR motion correction, and PET denoising (Armanious et al., 2020). An unsupervised dual-domain disentangled network (UDDN) was proposed to enhance the removal of rigid motion artifacts in MRI by leveraging both spatial and frequency information for improved efficacy (Wu et al., 2023).

Due to the difficulty in constructing paired datasets for motion artifact correction (i.e., motion-free and motion-corrupted images), various unsupervised learning-based models for motion correction have emerged recently. Predominantly, these unsupervised learning models for motion correction are based on the CycleGAN framework, an image translation method using cycle-consistency (Zhu et al., 2017). For example, Cycle-MedGAN was proposed, which is an enhanced framework for unsupervised image translation, expanding on the CycleGAN framework by integrating innovative cycle-perceptual and cycle-style loss functions (Armanious et al., 2019). It is capable of PET to CT translation as well as motion artifact correction. A method utilizing the bootstrap technique with a sampling mask has also been developed. This methodology corrects motion-corrupted k-space lines via a two-step process: initial random downsampling within k-space followed by replenishment leveraging the CycleGAN framework (Oh et al., 2021). The Dual-Domain Unsupervised Motion Artifacts Disentanglement Network (DUMAD-Net), an approach that addresses motion correction of the liver, without requiring paired datasets, was also proposed as an unsupervised method (Bai et al., 2022). This approach capitalizes on within-domain and cross-domain translations to instruct autoencoders in acquiring feature representation, while employing cycle consistency, thus framing motion correction as an image-to-image translation challenge. More details of these motion artifact correction approaches are given in a review paper (Spieker et al., 2024).

1.3. Our contributions

As aforementioned, CycleGAN has often been used for unsupervised learning for motion artifact correction. However, there were some problems in using vanilla CycleGAN, where two generators and two discriminators are trained simultaneously. First, the model of CycleGAN becomes heavy due to its four neural network sub-models, and there is a disadvantage that if one of the two generators is not well trained, the other generator is also not well trained (Oh et al., 2020). In fact, when CycleGAN is used for motion artifact correction, it was observed experimentally that the generator that converts from motion-free domain to motion-corrupted domain often fails to generate realistic motion artifacts and instead generates just vague and indistinct noise.

The second limitation is that it is possible to have multiple motion-corrupted images corresponding to a single motion-free image. This presents an inherently ill-posed problem, which complicates the computation of the cycle-consistency loss. For example, if an image with few motion artifacts goes through the generator G_1 and returns to the motion-corrupted domain via the other generator G_2, and if a lot of motion artifacts are added to the image, the generator G_1 would not be effectively trained in terms of calculating the cycle consistency loss between the original image (which has few motion artifacts) and the returned image (which has lots of motion artifacts).

To address these limitations, this paper has the following main contributions.

(1) We propose a novel method that integrates MR-physics-based motion artifact simulator. Inspired by optimal transport driven CycleGAN (OT-CycleGAN), which proved that the performance is better with a single pair of generator and discriminator, we substitute the generator converting from the motion-free to motion-corrupted domain with the MR physics-based motion artifact simulator (Oh et al., 2020).
(2) The proposed model enhances the cycle consistency loss regularization by adding a module that estimates the motion severity of the input image. This severity information is passed to the

simulator, resulting in a more stable calculation of cycle consistency loss.

(3) A unique advantage of the proposed model is its ability to perform both motion correction and motion severity measurement simultaneously, enhancing its utility in clinical applications.

(4) The proposed model demonstrates quantitatively and qualitatively good performance across a wider range of motion severities, compared to other unsupervised and supervised models. Its smaller network parameters and stable convergence of cycle consistency loss contribute to efficient training and robust results.

The proposed method can be described as a retrospective unsupervised generative model that is trained with ground-truth images, which are required for the supervised loss computation in the discriminator.

2. Methods

2.1. Dataset

We trained our neural network using 3D T1-weighted MRI data from Brain Volume (BRAVO) dataset, which was obtained at Seoul National University Hospital, Seoul, South Korea. The MRI scans were performed on a 3T SIGNA Premier MRI scanner (GE Healthcare) with an echo time (TE) of 2.77 ms, a repetition time (TR) of 6.86 ms, a flip angle of 10°, and a pixel bandwidth of 244 Hz/pixel. The sagittal image matrix size varied from 256 × 256 to 512 × 512 pixels, with an in-plane resolution of 0.90 × 0.90 and slice spacing of 1 mm. The third dimension of the images had a range of 144–380 slices. A total of 17,202 slices of brain MRI data from 79 clinical pediatric patients were included in the training and validation set, while 1410 slices from an additional eight clinical pediatric patients were used for the testing set. It is of note that all of these subject scans were utilized as motion-free reference data since they do not contain motion artifacts.

In addition to the simulated training, validation, testing set, in-vivo evaluation was performed using Magnetization-Prepared Rapid Gradient-Echo (T1 MPRAGE) images from five subjects in both stable and motion artifact-inducing states. The acquisition parameters for the T1 MPRAGE scans were as follows: TE was set at 2.97 ms, TR at 2100 ms, with a flip angle of 9°, and a pixel bandwidth of 180 Hz/pixel. It is of note that the in-vivo data was exclusively used for inference, meaning the proposed model, trained entirely on simulated data, was tested using in-vivo data to further validate its robustness and applicability.

2.2. Motion artifact simulation

Due to the lack of data containing actual motion artifacts, the training data consisted of both motion artifact-free and simulated motion artifacts. Consequently, the label images of the motion-corrupted domain exist in the dataset of the motion-free domain. However, we note that during a single iteration, an image was independently sampled from each domain, thereby ensuring an unpaired training process. In order to generate the training dataset, an in-house rigid motion artifact simulation tool was applied to 87 motion-free subjects considering 2D sudden rotation and translation motions (Lee et al., 2020). In this study, to better apply the effects of motion severity regularization, our dataset largely contained sudden rigid motion, predominantly manifested as ringing and/or ghosting artifacts. The motion artifacts simulation was performed in two consecutive steps: (1) rotation motion was simulated in the image domain, and (2) translation motion was simulated by applying a phase shift in the k-space domain. This is to generate motion-corrupted data that closely mimics real artifacts by capturing both translation and rotation complexities, enabling more effective training and improving the reliability of the motion correction model. This simulation process allowed for the creation of a dataset that includes simulated motion artifacts, which can be used to train the network to better handle motion artifacts in the acquired images. The detailed process of the motion artifact simulation is illustrated in Fig. 1.

To calculate the motion severity regularized cycle consistency loss, we generated motion corrupted dataset with five levels of severity using the motion artifact simulator. The levels, with grades ranging from 1 to 5, were determined based on the amplitude of motion, number of corrupted TRs per motion, and number of motions in a full scan, which were set according to a discrete uniform distribution (Kecskemeti and Alexander, 2020). Details of our motion artifact simulation parameters are described as Table 1.

Where g is the motion severity level, ranges from 1 to 5, with higher values indicating a more severe level of motion. Based on the above details, across all levels of motion severity, the amplitudes of the translation and rotation motion were set in the range of 0–9 (pixel for translation and ° for rotation) for simulation, and the time required for one motion was set in the range of 1–5 per TR. Also, the number of movements in one 2D scan was set from 1 to 12. These conditions were determined numerically and empirically. The process of simulating motion artifacts can be summarized as follows. For each motion severity level, varying degrees of rotation, ranging from 0^o to 9^o, were applied in the image domain. The deformed image was then transformed into the k-space domain using Fourier transform where translation motion was simulated by introducing linear phase shifts in the phase-encoding direction, with shifts ranging from 0 to 9 mm. This process was repeated N times, where N represents the number of corrupted lines in k-space. Each severity level affected a specific range of k-space lines per motion repetition (TR). For instance, at a low motion severity level ($g = 1$), only one k-space line per TR was corrupted, whereas at a high severity level ($g = 5$), a range of 1–5 lines per TR were distorted. The accumulated effects of both rotation and translation motions produced the corrupted k-space, and the final motion-corrupted image was generated by applying the inverse Fourier transform to this data. Further details on the motion simulation tool can be found in our previous work (Lee et al., 2020), where the tool is made publicly accessible at https://github.com/Yonsei-MILab/MRI-Motion-Artifact-Simulation-Tool. In clinical practice, images with high motion severity level (i.e. beyond level 5) are typically re-scanned, rather than being restored or processed (Sreekumari et al., 2019). So, in order to exclude severely degraded images from the training set, we ensured that the autocalibration signal (ACS) lines (in this study, 36 lines) of the k-space did not contain any motion artifacts in all datasets. In clinical practice, these k-space lines are typically acquired in the beginning of the scan, thereby reducing the possibility of motion during acquisition in these lines (Nguyen et al., 2001). Fig. 2 shows some examples of the simulated motion-corrupted images with different motion artifacts severity levels.

The resulting dataset of 17,202 slices has some overlap between adjacent grades due to the random generation process. However, visual inspection confirmed that the grades generally correspond to the appropriate level of motion severity. It is of note that since the dataset used in this study was acquired with Cartesian sampling, all experiments were conducted using Cartesian data and corresponding motion artifact simulations. However, to extend the model to other sampling trajectories, such as radial data, radial motion simulation would be required during the generation of the training dataset.

2.3. Proposed model architecture

In this work, we propose a retrospective unsupervised motion artifact correction approach that does not rely on external recordings, utilizing a Severity-based Regularized Cycle Consistency method. The proposed method builds upon CycleGAN with two key modifications. First, one of the generators in the original CycleGAN's forward and inverse paths was replaced with a motion artifact simulator, resulting in what we refer to as CycleGAN with simulator (version 1). The second modification introduced a motion severity regularization term into version 1, leading to CycleGAN with motion severity regularizer

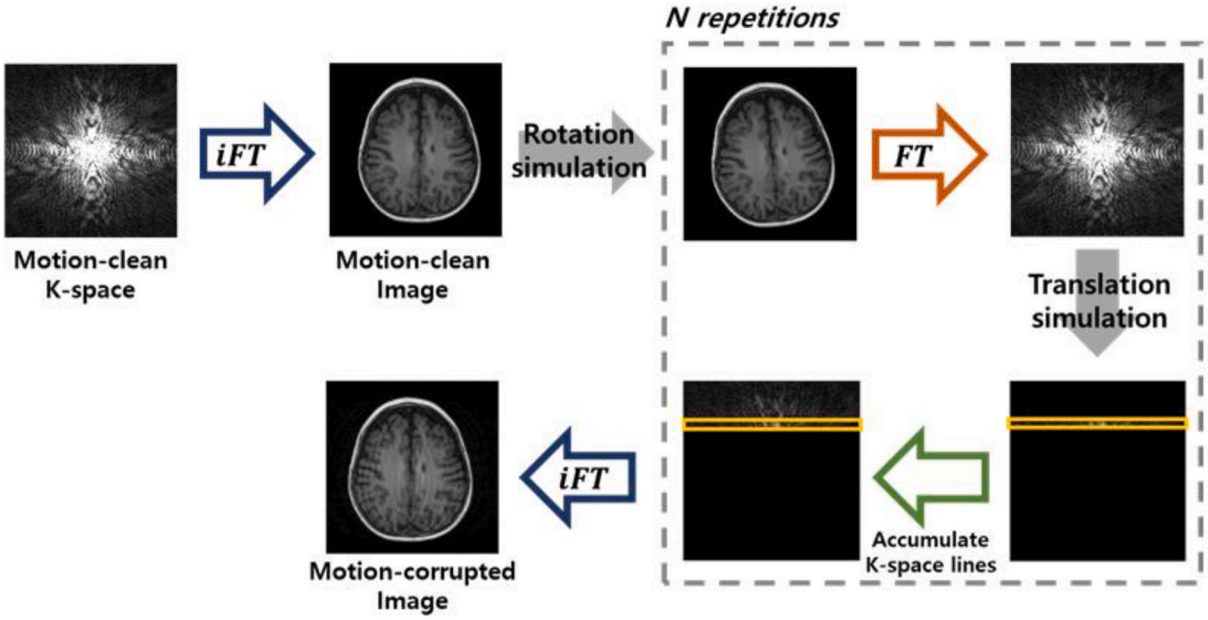

Fig. 1. Overview of the motion artifact simulation process, incorporating translation motion in the k-space domain and rotation motion in the image domain.

Table 1
The motion parameters corresponding to each motion grade.

Motion grade $\boldsymbol{g}$	1	2	3	4	5
Maximum amplitude of motion (*pixel*)	1	3	5	7	9
Maximum degree of rotation (°)	1	3	5	7	9
Number of corrupted K-space lines per 1 motion (*TR*)	1	1~2	1~3	1~4	1~5
Number of motions	1~4	3~6	4~8	5~10	7~12

(version 2). Fig. 3(a) illustrates the distinctions between the original CycleGAN and these two modified versions for clarity. The entire framework to train the proposed model is depicted in Fig. 3 (b). It consists of a generator (G), a discriminator (D), a motion artifact simulator (*sim*), and a motion severity estimator (E). The generator is a convolutional neural network based on Residual Network (ResNet). More structural details for all layers in both generator and discriminator are shown in Fig. 4. The generator consists of a two-layer encoder, nine residual blocks, a three-layer decoder, and a motion severity estimation module which has three residual blocks, three convolutional blocks, and a single fully connected layer. Each residual block contains two convolution blocks and a residual connection, where the convolutional block contains a convolution layer, an instance normalization layer, and the Rectified Linear Unit (ReLU). In addition, the discriminator is composed of five layers of convolutional blocks and can distinguish whether the motion-corrected images are real or fake.

To succinctly describe the training process: in the upper cycle, an image is randomly selected from the motion-corrupted domain and passed through generator G, resulting in a motion-corrected image and a predicted grade $\hat{g}$. Subsequently, these are fed into the motion artifact simulator to generate a motion-corrupted image anew and compute the initial image and cycle-consistency loss. Further, a cross entropy loss is calculated between the predicted grade $\hat{g}$ and the label grade g. Concurrently, in the lower cycle, an image is randomly selected from the

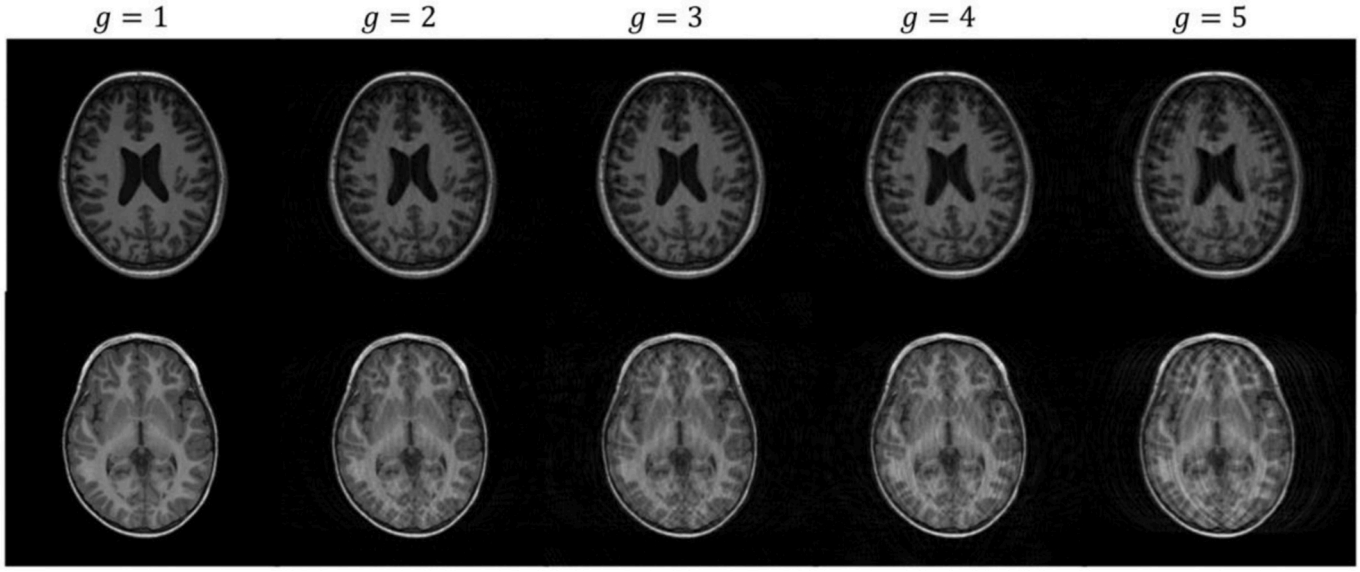

Fig. 2. Simulated data for different grades of motion severity. $\boldsymbol{g} = \mathbf{1}$ implies a little motion-corrupted data, while $\boldsymbol{g} = \mathbf{5}$ refers to the severe data.

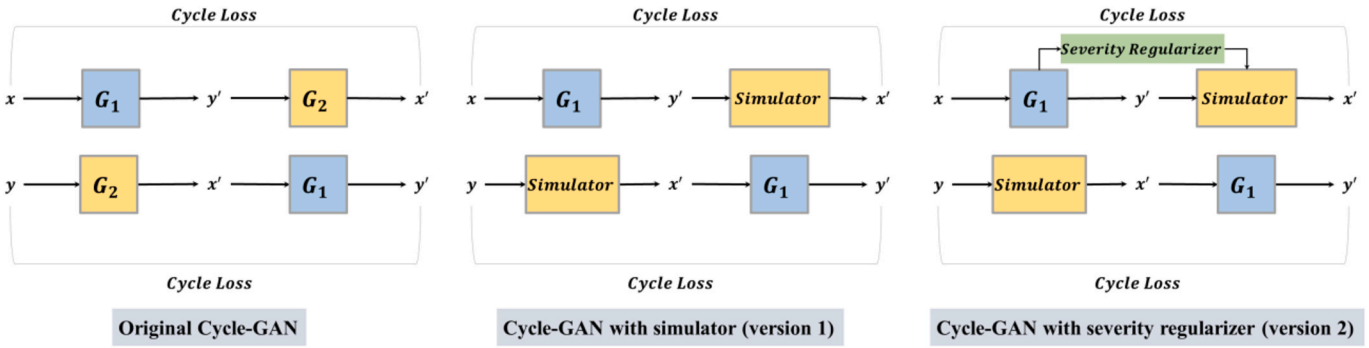

(a)

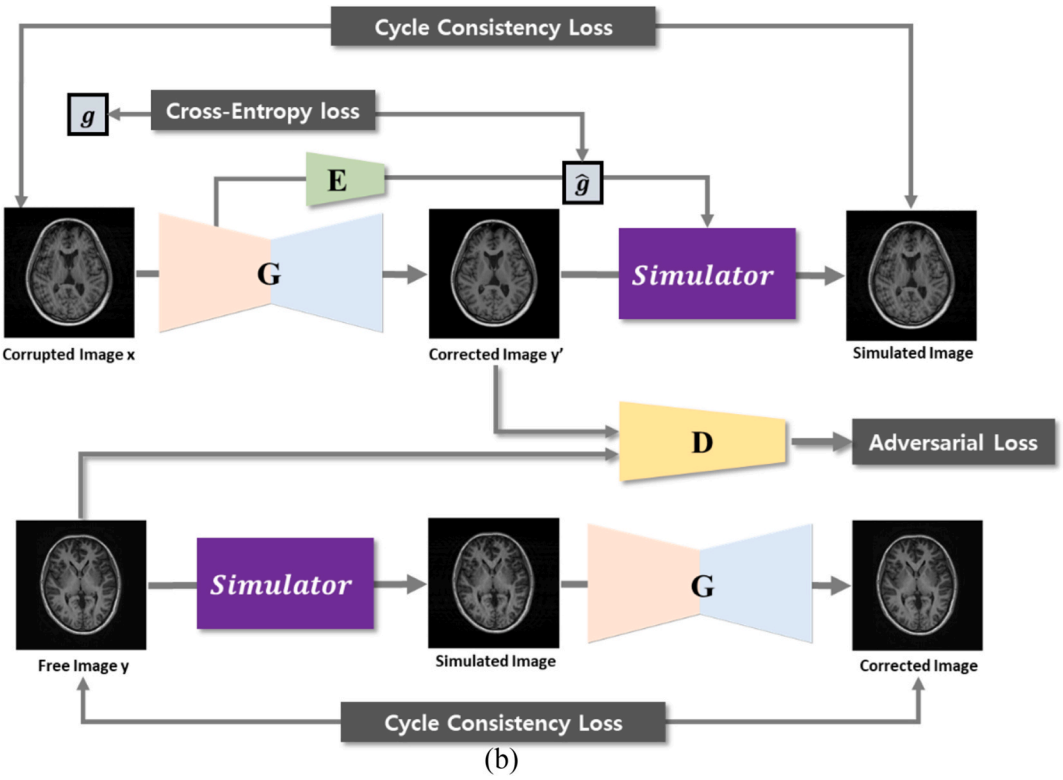

(b)

Fig. 3. (a) Key differences between the original CycleGAN and the proposed modifications: version 1 replaces one generator with a motion artifact simulator, while version 2 incorporates a motion severity regularizer. (b) An overview of the proposed motion correction method using modified CycleGAN (version 2).

motion-free domain, which also undergoes a similar process to compute the second cycle-consistency loss. An adversarial loss is also computed in the discriminator D, thereby complementing the overall training process.

2.4. Cycle consistency with motion severity regularization

Our motion correction network is based on CycleGAN, which converts images between motion-free domain and motion-corrupted domain. Central to this framework is the cycle consistency loss, which ensures that the images transformed from one domain to another and back retain their original content. This cycle consistency loss function can be expressed mathematically as follows.

$$\mathscr{L}_{cyc1}(G_1, G_2) = \mathbb{E}_{x\sim p_{data}(x)}[\|G_2(G_1(x)) - x\|_1] + \mathbb{E}_{y\sim p_{data}(y)}[\|G_1(G_2(y)) - y\|_1], \quad (1)$$

where G_1 and G_2 refer to the two generators that map images between the motion-corrupted domain and the motion-free domain. Here, x and y mean motion-corrupted images and motion-free images, respectively. The term $\|\cdot\|_1$ denotes the L1 norm, which measures the absolute differences between the original and reconstructed images.

In our modified approach, we substitute one of the generators with a motion artifact simulator, retaining only a pair of generators and discriminators. This results in a revised cycle consistency loss formulation:

$$\mathscr{L}_{cyc2}(G) = \mathbb{E}_{x\sim p_{data}(x)}[\|Sim(G(x)) - x\|_1] + \mathbb{E}_{y\sim p_{data}(y)}[\|G(Sim(y)) - y\|_1], \quad (2)$$

where *Sim* refers to an MR physics-based motion artifact simulator, which randomly generates artifacts within the conditions specified for the entire dataset. This formulation ensures that the generated images, when processed through the simulator, should closely match the original motion-corrupted images, thereby enforcing consistency between the domains.

To enhance training stability and improve the accuracy of motion artifact correction, we incorporate motion severity regularization. This updated cycle consistency loss is expressed as:

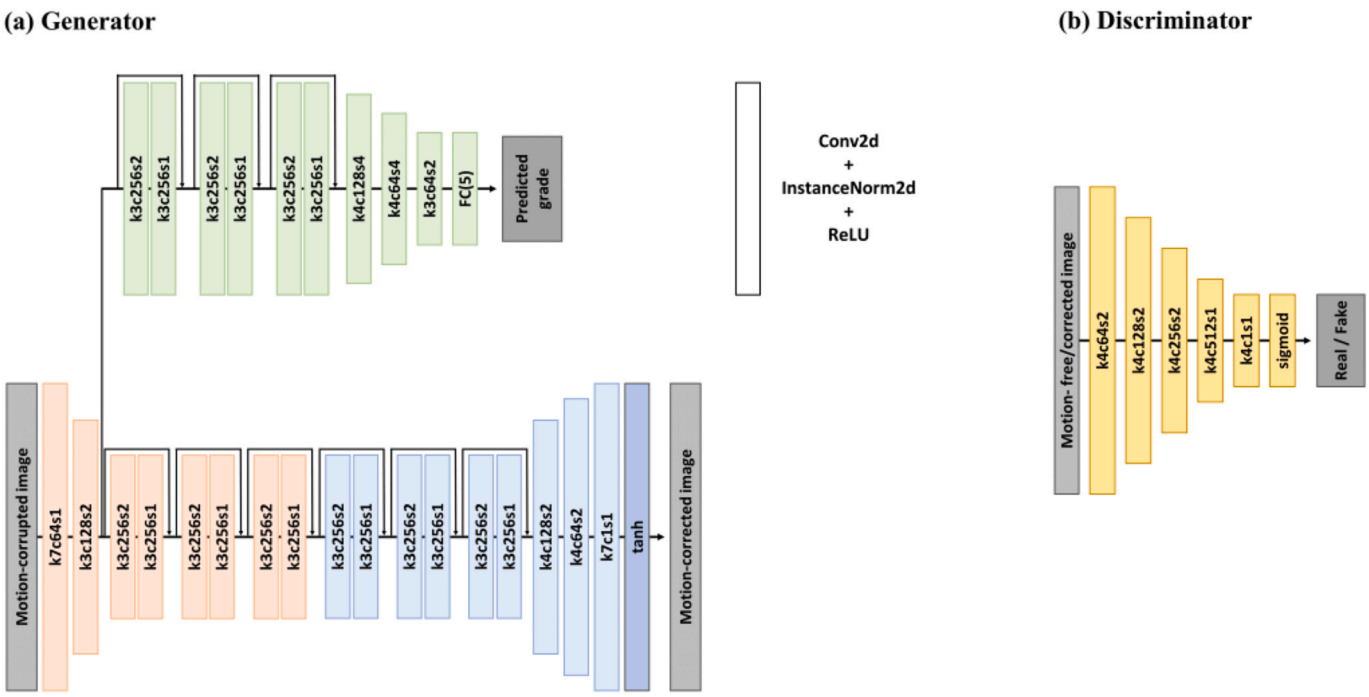

Fig. 4. Details of the network architecture used in the proposed model.

$$\hat{y}, \hat{l} = G(x),$$

$$\mathscr{L}_{cyc3}(G) = \mathbb{E}_{x\sim p_{data}(x)}[\|Sim(\hat{y}, \hat{l}) - x\|_1] + \mathbb{E}_{y\sim p_{data}(y)}[\|G(Sim(y, l)) - y\|_1], \tag{3}$$

where $\hat{y}$ refers to a motion-corrected image generated by G. l and $\hat{l}$ refer to estimated motion severity level (in form of one-hot vector from g and $\hat{g}$) and its corresponding severity level, respectively. Unlike the previous case, G was designed to give $\hat{y}$ and $\hat{l}$ as outputs and *Sim* refers to an MR physics-based motion artifact simulator, which takes a motion-free image and a motion severity level as input. This approach aims to ensure that the motion severity information is consistently integrated into the simulation process.

Furthermore, in order to train the motion severity assessment module in the generator, a cross-entropy loss was calculated between the predicted motion severities and the ground-truth motion severities that were utilized in the generation of the dataset.

$$\mathscr{L}_{sev}(G) = -\sum_{i=1}^{5} l_i \log(\hat{l}_i), \tag{4}$$

where l_i and $\hat{l}_i$ refer to i^{th} elements of label and predicted motion severity level in form of one-hot vectors, respectively. By incorporating these detailed cycle consistency and motion severity regularization losses, our model achieves more accurate motion artifact correction and improves the overall stability of the training process.

2.5. Other loss functions

In this work, we included an identity loss that trains the generator to generate motion-free images as its output, given motion-free images as input. It can be written as follows.

$$\mathscr{L}_{identity}(G) = \mathbb{E}_{y\sim p_{data}(y)}[\|G(y) - y\|_1]. \tag{5}$$

Since there is only one generator and the other generators have been replaced by model-based simulators, only one identity loss needs to be calculated. As previously stated, because one generator was replaced with a motion artifact simulator based on MR physics, our model includes only one single generator and discriminator. So, unlike the original CycleGAN, our model has only one adversarial loss as follows.

$$\mathscr{L}_{GAN}(G, D) = \mathbb{E}_{y\sim p_{data}(y)}[logD(y)] + \mathbb{E}_{x\sim p_{data}(x)}[\log\,(1 - D(G(x))], \tag{6}$$

where generator G tries to generate the realistic motion-free image while discriminator D tries to distinguish the fake motion-corrected image generated by G. Finally, our total loss is:

$$\mathscr{L}(G, D) = \mathscr{L}_{GAN}(G, D) + \lambda_{identity}\mathscr{L}_{identity}(G) + \lambda_{sev}\mathscr{L}_{sev}(G) + \lambda_{cyc}\mathscr{L}_{cyc3}(G), \tag{7}$$

where λ s are weights of each loss. Our training proceeds in the direction of solving the following equation:

$$G^* = arg\min_G \max_D \mathscr{L}(G, D). \tag{8}$$

2.6. Implementation

All images used for our training were normalized between 0 and 1. The λ values were determined heuristically by testing multiple configurations and selecting the one that produced the best results. The optimal results were obtained with minimal weighting for the identity loss ($\mathscr{L}_{identity}$) and motion severity assessment loss ($\mathscr{L}_{sev}$), both set at $\lambda_{identity} = \lambda_{sev} = 1$. However, to maintain the balance, the cycle consistency loss ($\mathscr{L}_{cyc3}$) was assigned a higher weight of $\lambda_{cyc} = 10$, ensuring its dominant contribution to the total loss and enhancing model performance. The model was trained for 150 epochs with batch size of 8, utilizing learning rate of 0.0002. The selection of 150 epochs was based on observing the training loss convergence during experimentation. Beyond this point, no significant improvements were observed in the validation performance, indicating that the model had effectively learned the underlying patterns. The Adaptive Moment Estimation (ADAM) optimizer was utilized with beta value of 0.5, and the exponentialLR scheduler was set with gamma value of 0.9. We selected the ADAM optimizer for its ability to handle sparse gradients in noisy problems, making it particularly suitable for training deep learning models on complex data such as motion-corrupted MRI images. In

addition, its adaptive learning rate helps to enhance convergence speed and overall model performance. All training procedures were implemented using the Nvidia RTX A5000.

2.7. Evaluation

Our experimental results can be broadly classified into three key categories. Firstly, we conducted performance evaluation of our model on simulated data. Secondly, we compared the performance of our model with other existing models. Finally, motion correction results were evaluated using separately acquired in-vivo data. To evaluate motion artifact correction quantitatively, we utilized evaluation metrics such as Mean Squared Error (MSE), Structural Similarity Index (SSIM), and Peak Signal to Noise Ratio (PSNR). It is important to acknowledge that the three metrics used in this study do not necessarily represent a definitive measure of motion correction performance. While a higher value of these indicators may suggest a superior image quality, this is not always the case. We also included the Feature Similarity Index (FSIM), which incorporates phase congruency (PC) and gradient magnitude (GM), both of which are well-suited for assessing image quality in tasks like MRI motion artifact correction. Specifically, PC captures perceptually significant local structures, while GM reflects local intensity variations, providing a robust basis for evaluating image quality (Zhang et al., 2011). Furthermore, to assess the blur degree in the resultant images, we employed a no-reference perceptual blur metric, which is an indicator that suggests an escalation in blur as the metric value augments (Crete et al., 2007). Additionally, an expert radiologist performed a qualitative evaluation of the motion-corrected images from both simulated data and in-vivo tests.

3. Results

3.1. Effect of motion severity regularization

To evaluate the effect of our motion severity regularization, we compared the performance of three scenarios on the simulated dataset: 1) the original CycleGAN, 2) a model that replaced one generator with a motion artifact simulator, and 3) a model that included motion severity regularization term. According to the results presented in Table 2, the average SSIM of the motion-corrupted simulation dataset was 0.757. After applying motion correction using the original CycleGAN, the average SSIM value improved to 0.931. Replacing one generator with a motion simulator (version1) slightly enhanced the performance, resulting in an average SSIM value of 0.942. Our final proposed model, which included motion severity regularization (version2), demonstrated the highest average SSIM of 0.961. PSNR showed the same trend as SSIM, whereas MSE showed the opposite trend. As previously mentioned, the generator and discriminator were removed one by one, the number of parameters in version1 was only half that of the original CycleGAN. However, due to the addition of the motion severity assessment module for motion severity regularization, the number of parameters in version2 slightly increased compared to version1. In conclusion, the proposed optimized CycleGAN with motion severity regularization significantly enhances motion artifact reduction, achieving improvements of 20.4%, 4.2%, 12.5%, and 59.5% in terms of SSIM, FSIM, PSNR, and MSE, respectively, compared to the corrupted simulation data.

Table 2
Ablation experiments on the impact of motion artifact simulator and motion severity regularization term compared to the original CycleGAN.

Experiment	SSIM	PSNR	MSE	FSIM	#Parameters (M)
Corrupted Simulation Data	0.757	31.16	50.14	0.933	–
CycleGAN	0.931	31.72	43.86	0.970	28.3
CycleGAN with Simulator (version1)	0.944	33.49	31.11	0.975	14.1
CycleGAN with Motion Severity Regulaizer (version2)	0.961	35.07	20.32	0.975	19.0

Fig. 5 demonstrates a boxplot graph plotting the SSIM values according to the severity of motion in five levels. This graph compares the SSIM values of motion-corrupted data, motion correction results of the original CycleGAN, and the motion correction results of the proposed model that includes our suggested regularization. From the graph, it is evident that the proposed model outperforms the original CycleGAN in all five levels of motion severity.

Qualitatively, as shown in Fig. 6, it can be asserted that our proposed optimized CycleGAN version 2 demonstrated the most effective correction compared to the other models. Although all models appeared to compensate adequately for grade 1 motion artifacts, a closer examination of the results reveals a slight difference. The proposed version 2 demonstrated sharper results and more closely resembled the ground-truth when compared to the original CycleGAN and version 1. As the severity of motion increased, it became increasingly evident that the proposed model outperformed the other models in correcting motion artifacts. Notably, in the case of grade 3 motion severity, the original CycleGAN demonstrated limited correction, whereas the proposed model effectively corrected almost all artifacts. However, for grade 4, which is the most severe, it can be observed that some motion artifacts remain in the results of the proposed model, albeit to a lesser degree than the other models. From these results, it can be inferred that the proposed model outperforms existing models across a broader range of motion severities.

Fig. 7 displays the confusion matrix that represent the performance of the motion artifact severity assessment module included into the proposed model. The accuracy for the total evaluation dataset was 86.1%. As mentioned in the dataset section, the proposed model was trained on dataset with incomplete labeling. Despite this limitation, the model demonstrated satisfactory performance.

3.2. Comparison against other models

To assess the performance of the proposed model, a comparative analysis was conducted against traditional methods, including FreeSurfer and Functional MRI of the Brain (FMRIB) Software Library (FSL), as well as deep learning-based motion correction models, such as MARC, Cycle-MedGAN, stacked U-Nets, UDDN, and pix2pix networks (Al-masni et al., 2022; Armanious et al., 2019; Isola et al., 2017; Tamada et al., 2020; Wu et al., 2023). The results demonstrate a significant improvement of our proposed model compared to the traditional methods, as illustrated in Fig. 8. This may be attributed to the fact that methods like FreeSurfer and FSL rely on predefined assumptions and rigid algorithms, which lack adaptability to diverse motion artifact patterns. As aforementioned, MARC is a supervised learning model that based on a conventional CNN for motion correction, while Cycle-MedGAN is an unsupervised learning model based on CycleGAN. All models were trained using the same dataset and their performances were evaluated through qualitative and quantitative comparisons, which are presented in Fig. 9 and Table 3, respectively. The proposed model shows better correction results than the unsupervised learning Cycle-MedGAN model, but it is slightly inferior to the supervised learning MARC model. The results of the quantitative analysis showed that MARC achieved the highest average SSIM and PSNR scores, likely due to its supervised learning approach with a paired dataset. However, the quantitative values were not much different from our proposed method (SSIM: 0.969 vs.0.961). Conversely, Cycle-MedGAN exhibited the poorest performance across all quantitative metrics. The observed difference in quantitative performance between Cycle-MedGAN and the proposed model, which also employs unsupervised learning, can be attributed to the motion severity regularization term, which enables the proposed model to cover a broader range of motion severities. The results show that while the UDDN model produces noticeably blurred images after

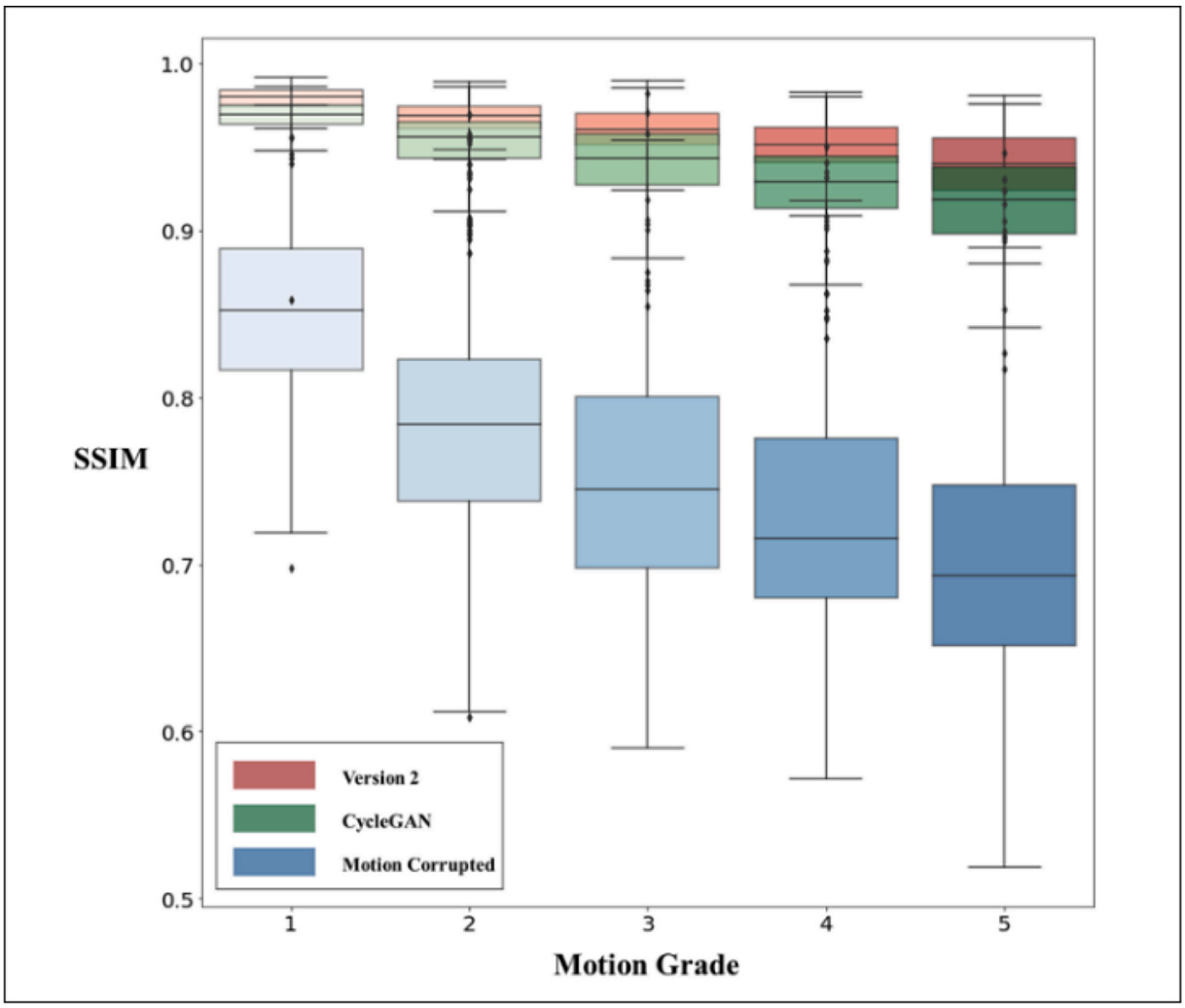

Fig. 5. Boxplot of SSIM values across five motion severity levels, comparing the performance of the proposed model with the original CycleGAN.

motion correction compared to the proposed method, the pix2pix network exhibited the worst blurring, with a blurring index of 0.631. This is further reflected in its FSIM score, indicating the lowest image quality even after artifact correction. In contrast, the proposed CycleGAN with Motion Severity Regularizer (version 2) achieves higher FSIM score of 0.975 compared to other methods, consistently improving motion correction performance over motion-corrupted images. These findings highlight the reliability and consistency of our method across different evaluation metrics.

Qualitatively, the comparison between MARC and the proposed model revealed an interesting observation. Despite MARC's superior quantitative indicators (SSIM, PSNR, MSE), the proposed model demonstrated better qualitative outcomes, as demonstrated in Fig. 9. Although the MARC model effectively corrects motion artifacts, the radiologist's evaluation noted increased image blurring and a plastic-like texture compared to the proposed method. This can be confirmed from the values of the blur metric introduced earlier. As evident from Table 3, the highest blur metric value was found to be associated with MARC, thereby further supporting our analysis.

3.3. In-vivo results

This section presents the motion correction results obtained from in-vivo data with real motion artifacts, rather than simulated motion artifacts. As mentioned in the dataset section, actual motion corrupted T1 MPRAGE data from five subjects were obtained. In addition, no-motion images from the same subjects were additionally acquired and used as reference images. The results of processing the in-vivo images through the proposed trained model are displayed in Fig. 10. Since the reference image is a rescanned image, there are cases where the slice number and the position or angle of the brain in the image are slightly different, but it can be seen that the proposed model corrects the real motion artifact. Furthermore, the proposed model demonstrated the ability to predict the grade of actual motion severity, with results that closely matched those assessed by visual inspection.

Fig. 11 shows the results of correcting motion artifacts in-vivo with the proposed model in three domains. Despite the model's training being confined to a 2D axial domain dataset, it is observed that the model is capable of effectively mitigating motion artifacts in images across the other two domains as well. However, in the sagittal and coronal domains, the presence of slight horizontal lines attributable to slice discrepancies in the axial direction is visible. This may represent a potential limitation of the present study. Despite this limitation, the radiologist's assessment indicated that the motion-corrected images enhanced anatomical and pathological interpretation.

4. Discussion

In this paper, we introduce an unsupervised motion correction method utilizing regularized cycle consistency, specifically designed to address motion severity. While various models based on CycleGAN have been explored for unsupervised learning in motion artifact correction,

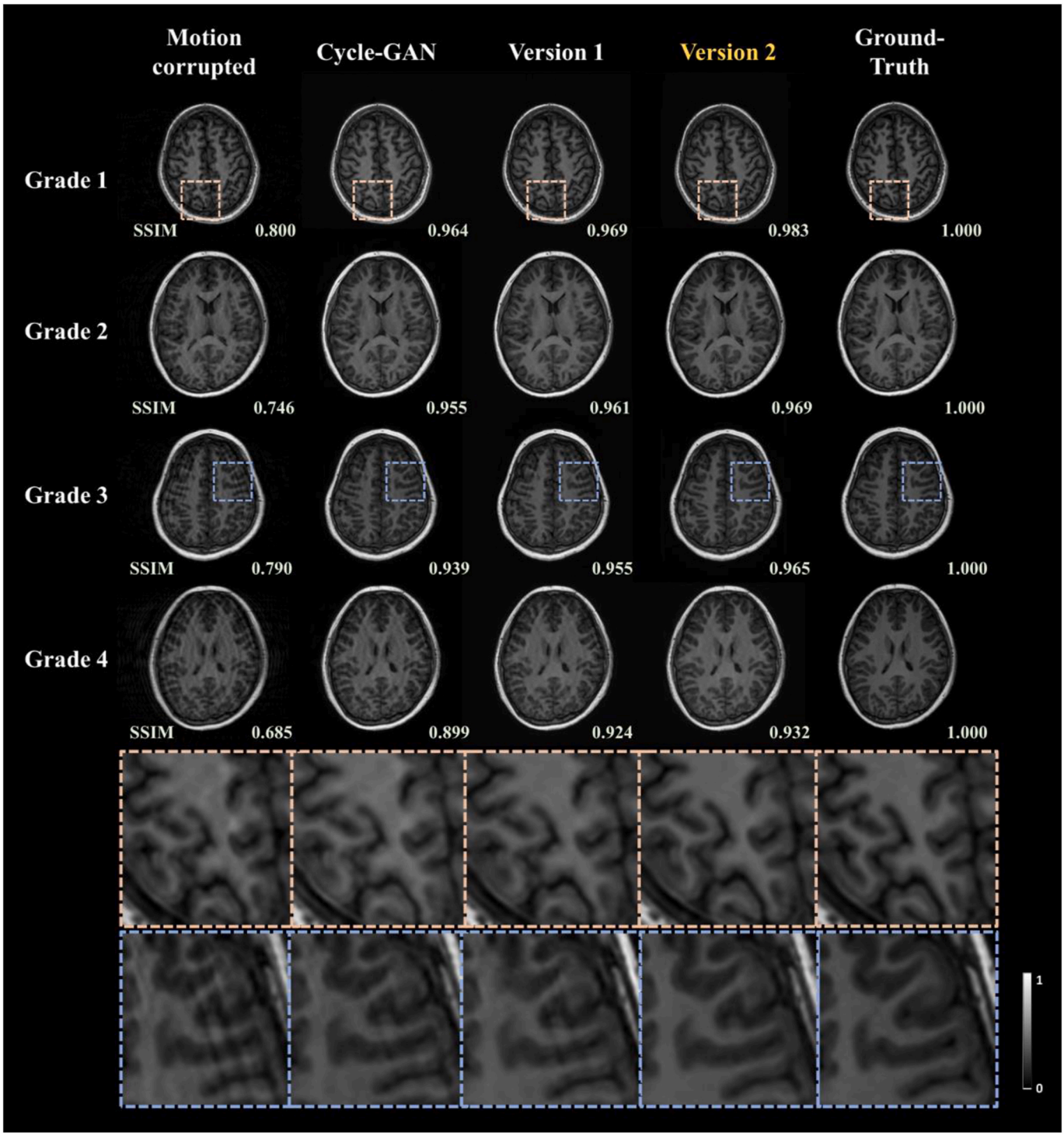

Fig. 6. Qualitative evaluation of various model versions across different motion levels using motion-simulated data.

they encountered notable challenges. Firstly, the generators tasked with synthesizing motion artifacts often struggled to produce realistic results, hampering training stability and overall progress. Secondly, an inherent ill-posedness arose due to the lack of one-to-one correspondence between images from motion-free and motion-corrupted domains.

To address these challenges, our proposed approach involved replacing one generator of CycleGAN with a physics-based motion artifact simulator and integrating a regularization term based on motion severity prior. This modification not only reduces the model's overall training complexity by decreasing the number of learnable parameters but also enhances the stability of cycle-consistency loss calculation.

Our proposed model exhibited superior quantitative and qualitative performance compared to the original CycleGAN and other existing unsupervised learning models for motion artifact correction. While it may yield slightly lower quantitative metrics compared to supervised learning models, it consistently generated clearer structural detail images. Specifically, our model achieved an SSIM of 0.961, an FSIM of 0.975, and an MSE of 20.32, outperforming the unsupervised CycleGAN with 0.931, 0.970, and 43.86, respectively, as well as Cycle-MedGAN with 0.941, 0.970, and 41.92. Additionally, our method yielded

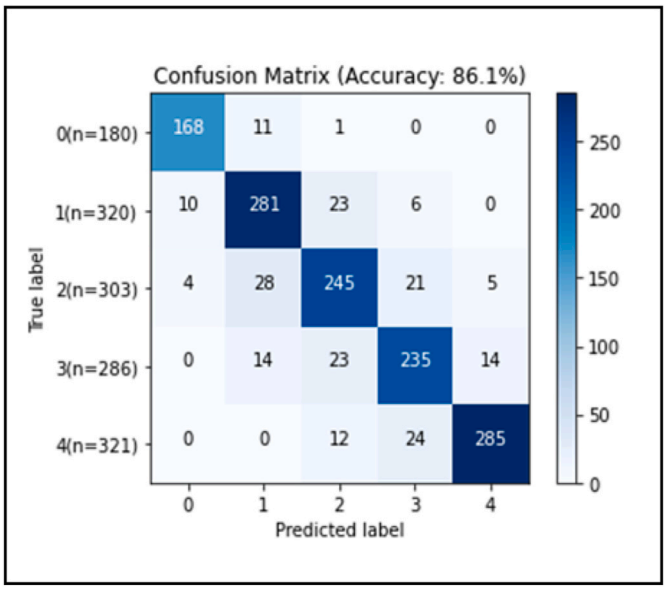

Fig. 7. Confusion matrix for motion severity assessment using the proposed model.

comparable quantitative results to supervised models, such as MARC, with a slight reduction in performance (SSIM of 0.961 vs. 0.969 and MSE of 20.32 vs. 20.11). However, our approach demonstrated a notable improvement in terms of the blurring index and FSIM, achieving 0.578 and 0.975 compared to 0.605 and 0.974 for MARC, respectively. Moreover, unlike other models whose performance deteriorated with widening motion severity ranges in the training dataset, our model maintained robust performance across all severity grades, demonstrating its effectiveness in handling variations in motion artifacts. In general, the proposed model demonstrates superior motion correction compared to other methods, attributed to the integration of an MR-physics-based motion artifact simulator. This approach enhances the cycle consistency loss by incorporating two additional modules: replacing one generator with the simulator and estimating motion artifact parameters during network training, thereby improving artifact correction.

The enhanced performance of our proposed model can be attributed to the integration of motion severity regularization, facilitating more accurate calculation of cycle consistency loss. Another perspective to consider is from the neural network standpoint, where the provision of additional motion severity information assisted in determining optimal correction parameters, leading to improved outcomes. This approach presented a robust and effective solution for MRI motion artifact correction, emphasizing the potential advantages of integrating supplementary data into deep learning models.

Moreover, our proposed model offered a unique advantage by simultaneously performing both motion correction and motion severity assessment. This dual functionality provided several clinical benefits, including reduced processing time, enhanced efficiency, and the ability to optimize correction outcomes based on real-time motion severity assessment.

The imaging dataset in this study was acquired from clinical pediatric patients from a clinical scanner. Therefore, all scans underwent acceleration (acceleration factor ranging from 2 to 3, depending on scan time). While accelerated imaging can help reduce motion artifacts by shortening acquisition times, pediatric patients are still prone to significant motion during scans. As a validation, we assessed the performance on both simulated corrupted data and real motion artifacts from in-vivo subjects. Our proposed optimized CycleGAN version 2 outperformed the original CycleGAN and MedGAN, and surpassed the supervised learning MARC method in blurriness metrics. Furthermore, expert radiologist has evaluated the performance of the proposed model, along with other state-of-the-art models, including Cycle-MedGAN and MARC. In Fig. 9, it is evident that the proposed model outperforms Cycle-MedGAN in terms of motion artifact correction. Although the supervised learning model, MARC, shows a similar level of motion artifact correction as the proposed model, it shows image blurring when compared to the proposed model. However, it is important to note that all proposed models exhibit slightly different gyration patterns compared to the ground-truth motion-free image. Fig. 10 illustrates the motion-corrected images obtained using the proposed model, demonstrating the effective elimination of motion artifacts. Nevertheless, upon comparison with the reference rescanned images, mild image blurring is observed. Fig. 11 displays coronal and sagittal reformatted images

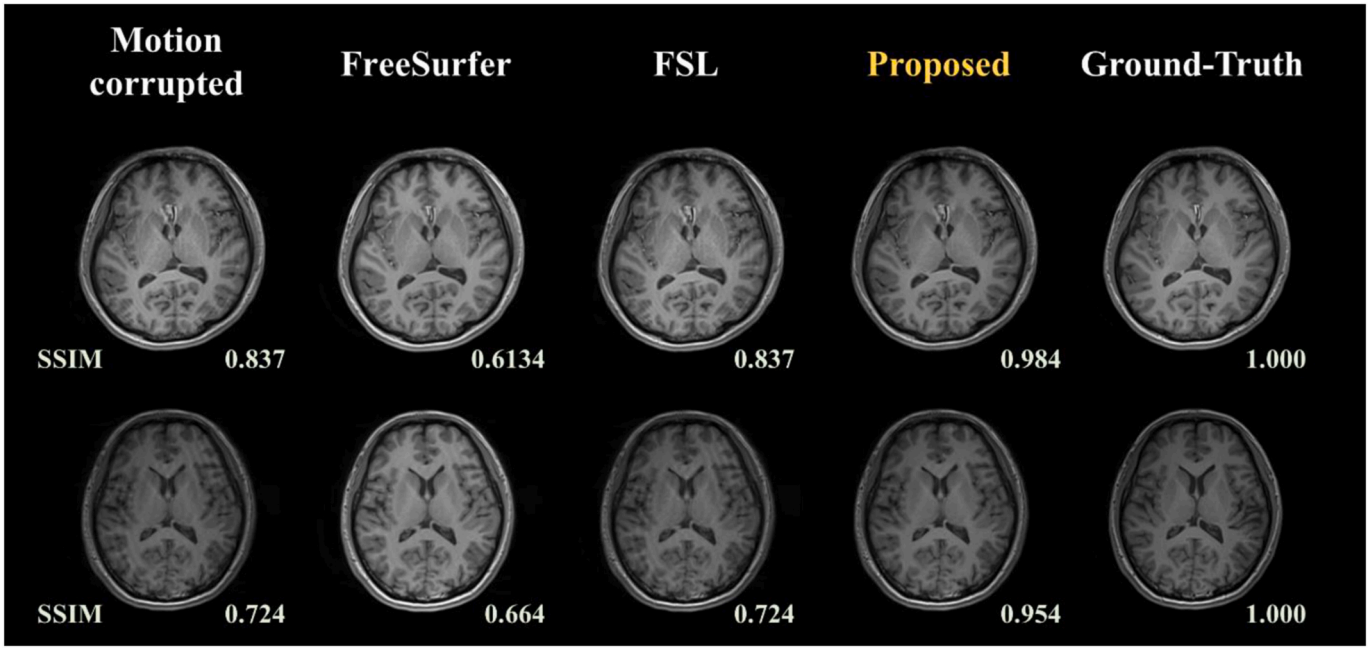

Fig. 8. Comparing the proposed model against traditional methods (FreeSurfer and FSL) for MRI motion artifact correction.

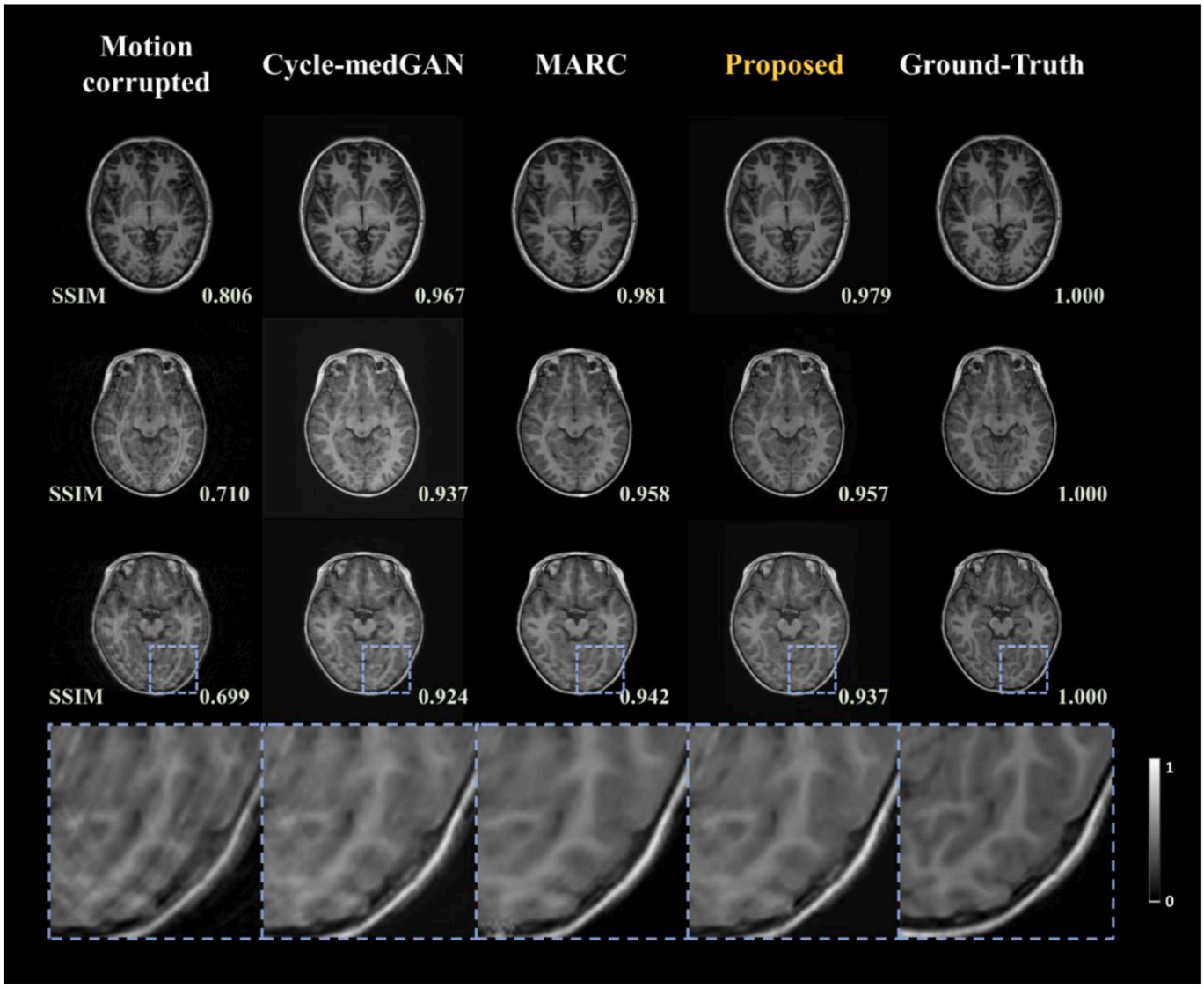

Fig. 9. Qualitative comparison of the proposed model with existing motion correction methods using motion-simulated data.

Table 3
Quantitative comparison against existing motion correction models.

Experiment	SSIM	PSNR	MSE	FSIM	Blur Index
Corrupted Simulation Data	0.757	31.16	50.14	0.933	–
pix2pix network (implemented)	0.808	29.55	46.13	0.927	0.631
UDDN (implemented)	0.849	31.41	41.03	0.952	0.608
Stacked U-Net (implemented)	0.902	33.05	37.31	0.964	0.583
Cycle-MedGAN (implemented)	0.941	33.12	41.92	0.970	0.584
MARC (implemented)	0.969	35.35	20.11	0.974	0.605
CycleGAN with Motion Severity Regularizer (version2)	0.961	35.07	20.32	0.975	0.578

revealing stair-step artifacts, a consequence of the proposed model being trained on a 2D axial image dataset. However, despite this limitation, the image quality of the reformatted images produced by the proposed model surpasses that of the motion-corrupted images.

During the in-vivo testing, we noted several restrictions. Our model operates in the 2D axial plane, and when these 2D motion-corrected slices are stacked to generate a 3D volume, interslice dependencies or stair-step artifacts can appear in the coronal and sagittal views. Another restriction is the lack of ground-truth rescan data without motion, which complicates the evaluation of our model's performance. Additionally, variations in motion artifacts, different imaging conditions, and scanning trajectories also introduce challenges to our proposed method for in-vivo testing.

This study has several limitations that need to be addressed in future research endeavors. Firstly, the proposed model was specifically designed to address certain types of motion artifacts. The motion severity regularization employed in our model relied on a motion artifact simulator, which can effectively handle only certain types of motion artifacts (specifically, 2D rigid and sudden motion artifacts in this study). Therefore, the range of motion artifacts that can be corrected is limited by the capability of the motion artifact simulator that has replaced the generator. To mitigate this limitation, future studies could explore the incorporation of additional information, such as a prior for motion artifact types like continuous and periodic motions.

The second limitation of this study pertains to the incomplete labeling of motion grades. Manually assessing motion severity ratings for a dataset comprising nearly 20,000 slices was practically unfeasible. Although we applied minimum conditions, such as defining the range of motion frequency and intensity, to each grade during dataset simulation, the simulation process was conducted randomly within these ranges. As a result, there was overlap in data between adjacent grades, potentially compromising the accuracy of motion severity assessment.

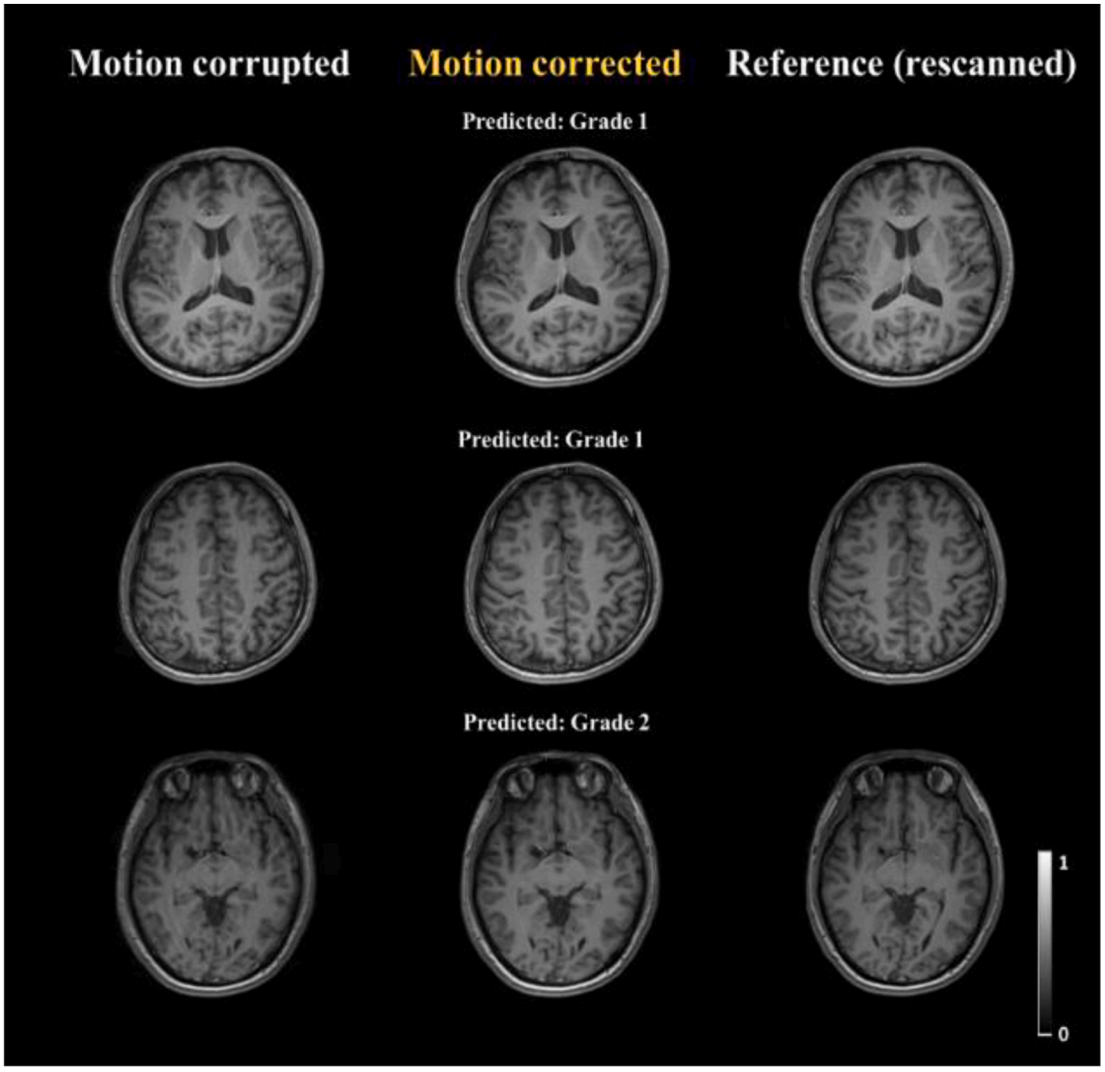

Fig. 10. Results of the proposed method applied to real motion in-vivo data. Reference images are rescanned images of the same subjects.

This study was conducted using simulations of rigid and sudden motion. However, incorporating non-rigid motion would introduce additional complexity and might necessitate a registration procedure before network training. Recent advancements in image translation techniques for handling misaligned training data could provide potential solutions for these challenges in future developments.

Nevertheless, this study presented a novel unsupervised learning model for MRI motion artifact correction, demonstrating superior performance compared to existing models while also enabling motion severity assessment. By overcoming limitations observed in traditional CycleGAN models, such as training instability and limited capability to handle diverse motion artifacts, our proposed model presented a more robust and effective approach to motion correction. Furthermore, the framework employed in this study, which involved replacing one of the generators in CycleGAN with a non-learnable model in the inverse direction, held promise for broader applicability beyond MRI motion correction. Thus, the findings of this study are expected to not only contribute to improving the efficacy of motion artifact correction in MRI but also provide a foundation for further research across various fields.

5. Conclusion

In this study, we present a novel unsupervised motion artifacts correction and assessment method using regularized cycle-consistency as severity. Notably, several shortcomings inherent in CycleGAN-based motion correction methodologies, such as ill-posed problems, were overcome by using a physics-based simulator and motion severity prior. The proposed model generally outperformed existing motion artifact correction models, suggesting the potential for further enhancements to our unsupervised learning model for MRI motion artifact correction. In addition, it was suggested that the proposed unsupervised learning model for motion artifact correction in MRI has potential for further improvements. One possible direction is using other types of regularization terms in addition to motion severity. Moreover, the framework used in this study, which replaces one of the generators in CycleGAN with a non-learnable model in the inverse direction, may be applicable to other fields beyond MRI motion correction. Therefore, the results of this study are expected to not only contribute to improving the performance of motion artifact correction in MRI, but also provide a foundation for further research in various fields.

CRediT authorship contribution statement

Seuk Kim: Writing – original draft, Methodology, Formal analysis, Data curation, Conceptualization, Software. **Mohammed A. Al-masni:** Writing – review & editing, Visualization, Supervision, Formal analysis, Conceptualization. **Seul Lee:** Validation, Software, Formal analysis, Data curation. **Sunyoung Jung:** Validation, Investigation, Formal

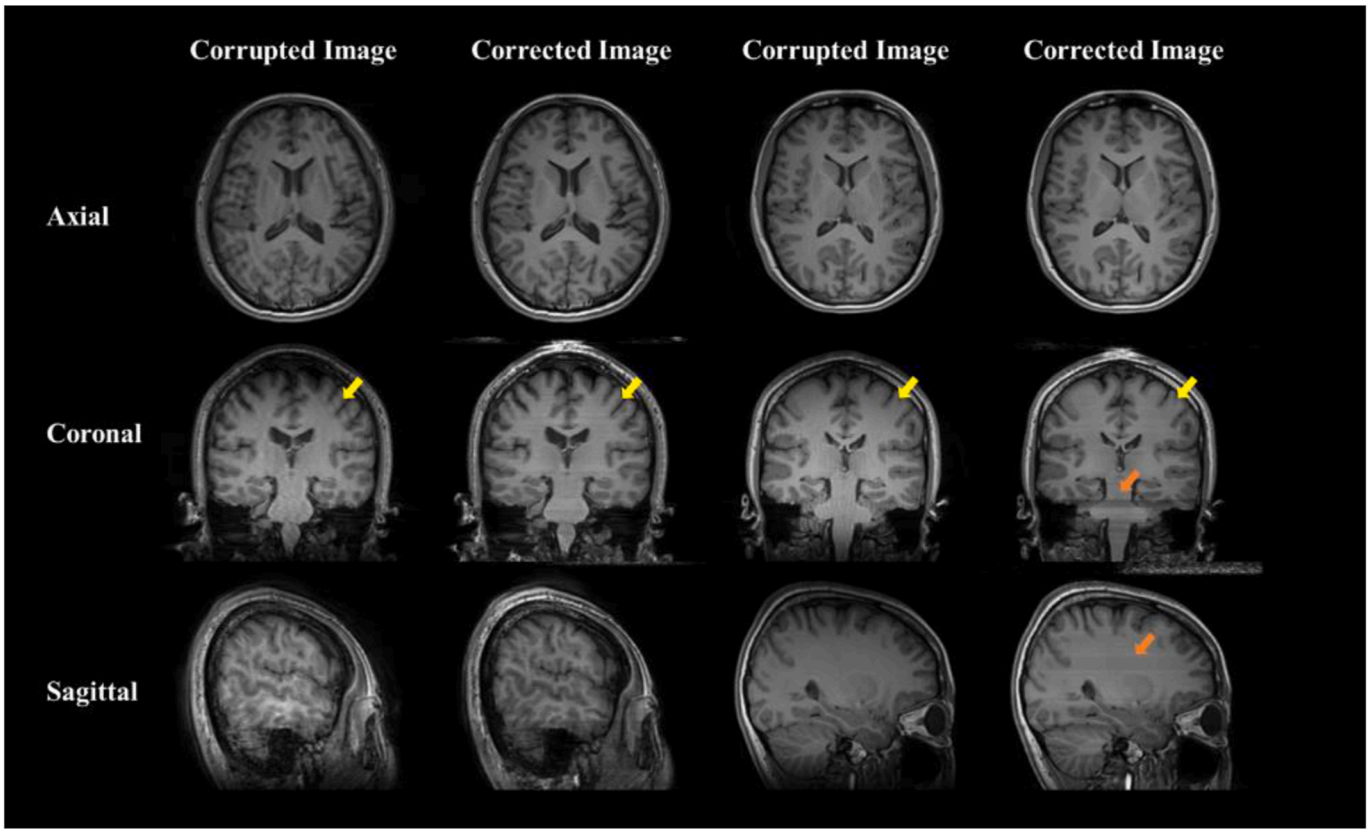

Fig. 11. Motion correction results in reformatted into the three domains.

analysis, Software. **Kyu-Jin Jung:** Visualization, Investigation, Data curation. **Chuanjiang Cui:** Validation, Formal analysis, Data curation. **Sung-Min Gho:** Validation, Methodology, Investigation, Formal analysis. **Young Hun Choi:** Validation, Investigation, Formal analysis, Data curation. **Dong-Hyun Kim:** Writing – review & editing, Supervision, Resources, Project administration, Funding acquisition, Conceptualization.

Declaration of competing interest

The authors declare that they have no known competing financial interests or personal relationships that could have appeared to influence the work reported in this paper.

Acknowledgement

This work was supported by the MSIT(Ministry of Science and ICT), Korea, under the ITRC(Information Technology Research Center) support program(IITP-2022-2020-0-01461) supervised by the IITP(Institute for Information & communications Technology Planning & Evaluation) and the Korea Medical Device Development Fund grant funded by the Korea government (the Ministry of Science and ICT, the Ministry of Trade, Industry and Energy, the Ministry of Health & Welfare, Republic of Korea, the Ministry of Food and Drug Safety) (Project Number: KMDF_PR_20200901_0062, 991006735). This work was also supported by the National Research Foundation of Korea (NRF) funded by the Korean government (MSIT) (No. RS-2023-00243034).

Data availability

The source code of our proposed is available at https://github.com/Yonsei-MILab/. However, the utilized data is not able to be made openly available due to the privacy issues of clinical data.

References

Al-masni, M.A., Lee, S., Al-Shamiri, A.K., Gho, S.-M., Choi, Y.H., Kim, D.-H., 2023. A knowledge interaction learning for multi-echo MRI motion artifact correction towards better enhancement of SWI. Comput. Biol. Med., 106553

Al-masni, M.A., Lee, S., Yi, J., Kim, S., Gho, S.-M., Choi, Y.H., Kim, D.-H., 2022. Stacked U-Nets with self-assisted priors towards robust correction of rigid motion artifact in brain MRI. Neuroimage 259, 119411.

Armanious, K., Jiang, C., Abdulatif, S., Küstner, T., Gatidis, S., Yang, B., 2019. Unsupervised medical image translation using cycle-MedGAN. 2019 27th European Signal Processing Conference (EUSIPCO). IEEE, pp. 1–5. A Coruna, Spain.

Armanious, K., Jiang, C., Fischer, M., Küstner, T., Hepp, T., Nikolaou, K., Gatidis, S., Yang, B., 2020. MedGAN: medical image translation using GANs. Comput. Med. Imag. Graph. 79, 101684.

Atkinson, D., Hill, D.L., Stoyle, P.N., Summers, P.E., Keevil, S.F., 1997. Automatic correction of motion artifacts in magnetic resonance images using an entropy focus criterion. IEEE Trans. Med. Imag. 16, 903–910.

Bai, C., Liu, K., Chen, S., Li, Z., Xie, W., Bao, Q., Liu, C., 2022. Dual-domain unsupervised network for removing motion artifact related to Gadoxetic acid-enhanced MRI. Journal of Physics: Conference Series. IOP Publishing, 012037.

Bosak, E., Harvey, P.R., 2001. Navigator motion correction of diffusion weighted 3D SSFP imaging. Magnetic Resonance Materials in Physics, Biology and Medicine 12, 167–176.

Cordero-Grande, L., Teixeira, R.P.A., Hughes, E.J., Hutter, J., Price, A.N., Hajnal, J.V., 2016. Sensitivity encoding for aligned multishot magnetic resonance reconstruction. IEEE Transactions on Computational Imaging 2, 266–280.

Crete, F., Dolmiere, T., Ladret, P., Nicolas, M., 2007. The blur effect: perception and estimation with a new no-reference perceptual blur metric. Human Vision and Electronic Imaging XII. SPIE, pp. 196–206.

Dou, Q., Feng, X., Wang, Z., Weller, D., Meyer, C., 2019. Deep Learning Motion Compensation for Cartesian and Spiral Trajectories. ISMRM Scientific Meeting & Exhibition.

Duffy, B.A., Zhang, W., Tang, H., Zhao, L., Law, M., Toga, A.W., Kim, H., 2018. Retrospective correction of motion artifact affected structural MRI images using deep learning of simulated motion. Medical Imaging with Deep Learning.

Godenschweger, F., Kägebein, U., Stucht, D., Yarach, U., Sciarra, A., Yakupov, R., Lüsebrink, F., Schulze, P., Speck, O., 2016. Motion correction in MRI of the brain. Phys. Med. Biol. 61, R32.

Haskell, M.W., Cauley, S.F., Wald, L.L., 2018. TArgeted Motion Estimation and Reduction (TAMER): data consistency based motion mitigation for MRI using a reduced model joint optimization. IEEE Trans. Med. Imag. 37, 1253–1265.

Herbst, M., Maclaren, J., Weigel, M., Korvink, J., Hennig, J., Zaitsev, M., 2012. Prospective motion correction with continuous gradient updates in diffusion weighted imaging. Magn. Reson. Med. 67, 326–338.
Hewlett, M., Petrov, I., Johnson, P.M., Drangova, M., 2024. Deep-learning-based motion correction using multichannel MRI data: a study using simulated artifacts in the fastMRI dataset. NMR Biomed. e5179.
Isola, P., Zhu, J.-Y., Zhou, T., Efros, A.A., 2017. Image-to-image translation with conditional adversarial networks. Proceedings of the IEEE Conference on Computer Vision and Pattern Recognition, pp. 1125–1134.
Johnson, P.M., Drangova, M., 2018. Motion correction in MRI using deep learning. Proceedings of the ISMRM Scientific Meeting & Exhibition, Paris, pp. 1–4.
Kecskemeti, S.R., Alexander, A.L., 2020. Test-retest of automated segmentation with different motion correction strategies: a comparison of prospective versus retrospective methods. Neuroimage 209, 116494.
Kromrey, M.-L., Tamada, D., Johno, H., Funayama, S., Nagata, N., Ichikawa, S., Kühn, J.-P., Onishi, H., Motosugi, U., 2020. Reduction of respiratory motion artifacts in gadoxetate-enhanced MR with a deep learning–based filter using convolutional neural network. Eur. Radiol. 30, 5923–5932.
Küstner, T., Armanious, K., Yang, J., Yang, B., Schick, F., Gatidis, S., 2019. Retrospective correction of motion-affected MR images using deep learning frameworks. Magn. Reson. Med. 82, 1527–1540.
Lee, J.Y., Seo, H., Lee, W.N., Park, H., 2024. Unsupervised motion artifact correction of turbo spin-echo MRI using deep image prior. Magn. Reson. Med. 92, 28–42.
Lee, S., Jung, S., Jung, K.-J., Kim, D.-H., 2020. Deep learning in MR motion correction: a brief review and a new motion simulation tool (view2Dmotion). Investigative Magnetic Resonance Imaging 24, 196–206.
Liu, J., Kocak, M., Supanich, M., Deng, J., 2020. Motion artifacts reduction in brain MRI by means of a deep residual network with densely connected multi-resolution blocks (DRN-DCMB). Magn. Reson. Imag. 71, 69–79.
Loizillon, S., Bottani, S., Maire, A., Ströer, S., Dormont, D., Colliot, O., Burgos, N., Init, A. D.N., Grp, A.S., 2024. Automatic motion artefact detection in brain T1-weighted magnetic resonance images from a clinical data warehouse using synthetic data. Med. Image Anal. 93.
Nguyen, T.D., Ding, G., Watts, R., Wang, Y., 2001. Optimization of view ordering for motion artifact suppression. Magn. Reson. Imag. 19, 951–957.
Oh, G., Jung, S., Lee, J.E., Ye, J.C., 2024. Annealed score-based diffusion model for MR motion artifact reduction. IEEE Transactions on Computational Imaging 10, 43–53.
Oh, G., Lee, J.E., Ye, J.C., 2021. Unpaired MR motion artifact deep learning using outlier-rejecting bootstrap aggregation. IEEE Trans. Med. Imag. 40, 3125–3139.
Oh, G., Sim, B., Chung, H., Sunwoo, L., Ye, J.C., 2020. Unpaired deep learning for accelerated MRI using optimal transport driven CycleGAN. IEEE Transactions on Computational Imaging 6, 1285–1296.
Pawar, K., Chen, Z., Shah, N.J., Egan, G.F., 2018. MoCoNet: motion correction in 3D MPRAGE images using a convolutional neural network approach. arXiv preprint arXiv:1807.10831. https://arxiv.org/abs/1807.10831.
Pawar, K., Chen, Z., Shah, N.J., Egan, G.F., 2022. Suppressing motion artefacts in MRI using an Inception-ResNet network with motion simulation augmentation. NMR Biomed. 35 (4), e4225.
Shaw, R., Sudre, C.H., Varsavsky, T., Ourselin, S., Cardoso, M.J., 2020. A k-space model of movement artefacts: application to segmentation augmentation and artefact removal. IEEE Trans. Med. Imag. 39, 2881–2892.
Spieker, V., Eichhorn, H., Hammernik, K., Rueckert, D., Preibisch, C., Karampinos, D.C., Schnabel, J.A., 2024. Deep learning for retrospective motion correction in MRI: a comprehensive review. IEEE Trans. Med. Imag. 43, 846–859.
Sreekumari, A., Shanbhag, D., Yeo, D., Foo, T., Pilitsis, J., Polzin, J., Patil, U., Coblentz, A., Kapadia, A., Khinda, J., Boutet, A., Port, J., Hancu, I., 2019. A deep learning-based approach to reduce rescan and recall rates in clinical MRI examinations. Am. J. Neuroradiol. 40, 217–223.
Tamada, D., Kromrey, M.-L., Ichikawa, S., Onishi, H., Motosugi, U., 2020. Motion artifact reduction using a convolutional neural network for dynamic contrast enhanced MR imaging of the liver. Magn. Reson. Med. Sci. 19, 64–76.
Tisdall, M.D., Hess, A.T., Reuter, M., Meintjes, E.M., Fischl, B., van der Kouwe, A.J., 2012. Volumetric navigators for prospective motion correction and selective reacquisition in neuroanatomical MRI. Magn. Reson. Med. 68, 389–399.
Vaillant, G., Prieto, C., Kolbitsch, C., Penney, G., Schaeffter, T., 2013. Retrospective rigid motion correction in k-space for segmented radial MRI. IEEE Trans. Med. Imag. 33, 1–10.
Wang, Z., Ran, M., Yang, Z., Yu, H., Jin, J., Wang, T., Lu, J., Zhang, Y., 2024. Generalizable MRI motion correction via compressed sensing equivariant imaging prior. IEEE Trans. Circ. Syst. Video Technol.
Wu, B., Li, C., Zhang, J., Lai, H., Feng, Q., Huang, M., 2023. Unsupervised dual-domain disentangled network for removal of rigid motion artifacts in MRI. Comput. Biol. Med. 165, 107373.
Zaitsev, M., Maclaren, J., Herbst, M., 2015. Motion artifacts in MRI: a complex problem with many partial solutions. J. Magn. Reson. Imag. 42, 887–901.
Zhang, L., Zhang, L., Mou, X.Q., Zhang, D., 2011. FSIM: a feature similarity index for image quality assessment. Ieee T Image Process 20, 2378–2386.
Zhu, J.-Y., Park, T., Isola, P., Efros, A.A., 2017. Unpaired image-to-image translation using cycle-consistent adversarial networks. Proceedings of the IEEE International Conference on Computer Vision, pp. 2223–2232.